1. Introduction

It is well known that tumour motion due to patient respiration has a detrimental effect on the therapeutic ratio, defined as TCP × (1 − NTCP), with TCP the tumour control probability and NTCP the normal tissue complication probability. Similar to uncertainties in, e.g., patient setup and target delineation, additional safety margins have to be applied to the clinical target volume (CTV) to ensure dosimetric coverage of this target. Applying additional margins may lead to increased dose to normal tissues, i.e. a higher NTCP. If the complication rate already limits the margins, intra-fractional breathing motion may reduce the probability of tumour control.

Geometric uncertainties in radiotherapy can be modelled as a combination of two components: systematic errors and random errors. Systematic errors can be thought of as treatment preparation errors, and result in a shift of the dose distribution with respect to the planned position. Random errors can be thought of as treatment execution errors, and result in a blurring of the dose distribution. Many authors have come up with recipes to determine necessary margins from CTV to planning target volume (PTV). A comprehensive overview of these recipes is given by van Herk (2004). Errors of the same type are generally added in quadrature, after which a margin recipe is applied to construct the required margin between CTV and PTV. All margin recipes in van Herk (2004) reflect that systematic errors are more important than random errors with a similar magnitude. Respiration-induced tumour motion has both a systematic effect and a 'random' effect:

- Patient respiration during CT-scanning results in distorted CT-images, leading to errors in the target shape and in the representative target position. This effect of patient breathing is well understood and either a strategy of slow-scanning (Lagerwaard *et al* 2001) or respiration-correlated CT-scanning (Ford *et al* 2003, Vedam *et al* 2003) will greatly improve target delineation.
- Even using a representative CT-scan, the patient can systematically breathe at a different level during treatment, introducing further systematic and random errors. Little is known about these kinds of errors but setting up the patient to the daily average tumour position, instead of using tattoos or bony anatomy, will eliminate the systematic component of respiration-induced errors. Image-guided radiotherapy, e.g., a strategy of real-time tumour tracking (RTRT), (Shirato *et al* 2000, Shirato *et al* 1999) or IRIS (Berbeco *et al* 2004), seems to be a prerequisite.
- Intra-fractional breathing motion has a blurring effect on the dose distribution. Image guidance is not necessary to minimize this blurring effect. Multiple non-image guided strategies (such as RPM (Varian Medical Systems), ABC (Wong *et al* 1999) and voluntary breath hold (Barnes *et al* 2001, Hanley *et al* 1999) using external respiratory monitors are available to freeze breathing motion, as well as RTRT and IRIS.

Methods for controlling patient respiration during treatment without image guidance are gradually finding their way into the clinic. When used during radiation delivery, they can, by their nature, only be used to minimize the blurring effect of respiration-induced tumour motion. Reports on the reproducibility of tumour position using deep-inspiration breath hold (DIBH) or gating, are promising. For example, Hanley *et al* (1999) report an inter-fraction and intra-fraction reproducibility of 2.5 and 1.0 mm (1SD), respectively. However, accurate data as to how much reduction in safety margins between CTV and PTV will be allowed using these techniques are scarce. Furthermore, since these techniques may be quite a strain on the patient, it may be worthwhile to determine for which patients these techniques are clinically relevant, depending on, e.g., the extent of the free breathing tumour motion.

In this paper we are only concerned with the blurring effect of respiration-induced tumour motion and will try to answer two questions.

(1) What margin should be applied for intra-fractional breathing motion, or how much can safety margins be reduced when controlling breathing motion during irradiation without changing the target coverage?
(2) Can intra-fractional breathing motion be modelled by a simple function with only the breathing amplitude as a parameter, allowing simple quadratic addition to other sources of random errors, despite the effects of baseline shifts and irregular breathing on the motion kernel?

This latter question is important since prior to treatment planning only very limited information with respect to the exact breathing motion is known. Often only an estimate of the peak-to-peak breathing motion is obtained by means of a fluoroscopy session or a time-resolved CT-scan. Some authors (Lujan *et al* 1999, Seppenwoolde *et al* 2002) have shown that it is possible to model tumour motion during a single breath with a certain power of the cosine function. This relationship may, however, very well break down when taking into account realistic breathing artefacts such as an irregular breathing amplitude or baseline drifting.

2. Materials and methods

Since breathing motion is usually most pronounced in the cranial–caudal direction, and for reasons of simplicity, we investigated the effect of intra-fractional breathing motion on the necessary safety margins in a one-dimensional simulation. Since blurring will have a larger effect on a steep dose gradient than on an already shallow dose gradient, both the situation of a penumbra (or dose gradient) in low-density lung tissue and in unit-density tissue were examined. For the same reason, we analysed whether the presence of inter-fractional random setup errors, which also leads to a more shallow dose gradient, alters the effect of intra-fractional breathing motion on the dose distribution.

The results from our analysis can either be used in a forward manner, i.e. to determine what margin should be applied to account for intra-fractional breathing motion when not controlling patient breathing during irradiation, or in a backward manner, i.e. to determine by how much the traditionally applied safety margins can be reduced when freezing tumour motion during irradiation. From now on we will simply refer to both options by 'the margin' for intra-fractional breathing.

2.1. What margin is affected by intra-fractional breathing motion?

In order to determine the margin for intra-fractional breathing motion, we need to define some quantity that has to stay constant when comparing the situations with and without this breathing motion. We define the following:

> The margin for intra-fractional breathing motion is the increase in margin between CTV and PTV necessary to ensure the same tumour coverage as without this intra-fractional motion.

This definition is clarified in figure 1, which is a one-dimensional example of the application of margins in radiotherapy as suggested by the ICRU (1993, 1999). In figure 1(a) it is assumed there is no intra-fractional breathing motion. To account for the possible spread of sub-clinical disease, a margin is applied to the gross tumour volume (GTV) yielding the CTV. Next, a margin is applied to the CTV to account for a combination of systematic

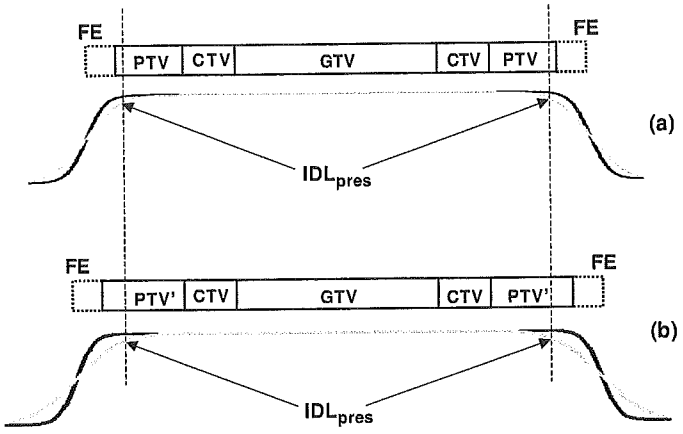

Figure 1. Schematic overview of margining from GTV to field edge (FE) without (a), and with (b) intra-fractional breathing motion. With breathing motion the prescribed isodose level will move farther inward due to blurring. For a consistent position of this isodose level after blurring, an increase in margin from CTV to PTV', and increase in field sizes, is necessary.

and random errors, yielding the planning target volume. The construction of an internal target volume (ITV, not shown in the figure) may be an intermediate step in constructing the PTV from the CTV. The goal of treatment planning is to conform a certain prescribed isodose level (IDL_{pres}) to this PTV. The solid black line indicates the planned one-dimensional dose distribution. The grey line is the dose distribution after blurring for, e.g., random setup errors. Using the probability based approach by van Herk *et al* (2000), this blurred dose distribution in combination with the distribution of systematic errors will result in some, as yet undefined, probability distribution of tumour coverage.

Now, *with* the presence of intra-fractional breathing motion, we would like to keep this probability of tumour control constant. To first order this can be achieved by ensuring the same position of IDL_{pres} after blurring (indicated by the vertical dashed line in figure 1). Since blurring now includes intra-fractional breathing motion, the displacement of IDL_{pres} with respect to the unblurred dose profile will be larger and therefore a larger margin from CTV to a new PTV (denoted as PTV') is needed (figure 1(b)). Note that the margin from the new PTV to the field edge is the same as in figure 1(a).

2.2. Real-time tumour tracking data

A popular model for breathing motion assumes that the respiration-induced tumour position as a function of time, $S(t)$, is described by

$$S(t) = S_0 - A\cos^{2n}(\pi t/T - \phi) \tag{1}$$

with S_0 the tumour position at exhalation, A the peak-to-peak breathing amplitude, T the period of the breathing cycle and ϕ the starting phase (Shirato *et al* 2004). n is a positive integer which usually has a value of 1 or 2 (Seppenwoolde *et al* 2002). For $n > 1$ this function does describe the fact that usually more time is spent at exhale than at inhale. However, Seppenwoolde *et al* report that for half of their patients a value of $n = 1$ is adequate. Furthermore, irregular breaths and base-line shifts make it impossible to describe respiration-induced tumour motion with a simple function. We therefore opted to use breathing data measured during real-time tumour tracking radiotherapy (RTRT) (Shirato *et al* (1999, 2000)) as performed now for a

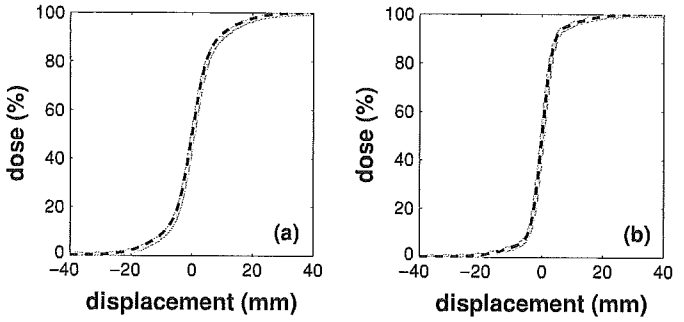

Figure 2. Dose profiles for an 8 MV photon beam in material of lung density (a) and unit density (b). The thick grey line is the measured data. The dashed black line is a fit with two error functions.

number of years at Hokkaido University. Forty patients (43 tumour locations) were treated to a total of 178 fractions. The 178 measured breathing traces were cleared of tracking errors and corrected for couch rotations in between fields resulting in breathing traces in the three cardinal directions, cranial–caudal (CC), left–right (LR) and anterior–posterior (AP). Each trace represented a single multiple field fraction with an average fraction time of 1400 s (data acquisition time: 700 s). The median peak-to-peak breathing amplitude (A, i.e. the median distance between subsequent exhale and inhale positions) for each direction was determined, and the direction with the largest A, usually the cranial–caudal direction, was selected for further analysis. A probability density function (PDF) of the tumour position over time was created with a bin width of 1 mm. Since we were only interested in the blurring effect of breathing, the PDF was shifted such that the average tumour displacement was zero. This assumes that patient set-up for each fraction is at the average tumour position which, in clinical practice, is hard to achieve. An average tumour position unequal to zero would, however, be a systematic error for that fraction and therefore falls outside of the scope of our study.

We would like to emphasize the following. Although we use breathing data acquired during RTRT, we do not use these data to assess the full potential of RTRT, but only to study the effect of controlling intra-fractional breathing motion (by means of, for example, ABC, RPM or voluntary breath hold). Next to minimizing the effects of breathing motion, RTRT also minimizes most of the (size of) systematic and random setup errors, which is not a part of the current study.

2.3. Blurring the dose profile

The dose profile of an 8 MV photon beam was measured using radiographic film in both cork (with a density of 0.25 g cm^{-3}, simulating tissue of lung density) and polystyrene (simulating unit-density tissue), see figure 2. To speed up calculations, the dose profiles were fitted with error functions (equation (2)). Two error functions provide an accurate fit for describing the dose D as a function of position x:

$$D = \frac{w_1 \mathrm{erf}\left(\frac{x}{b_1}\right) + w_2 \mathrm{erf}\left(\frac{x}{b_2}\right)}{2} \times 100 \qquad (2)$$

with w the relative weights and b the 'slope' of the respective error functions. The fitting values are provided in table 1. For simplicity we only used a one-sided dose profile, i.e. starting at a dose of zero at $-\infty$, 50% at position 0 and 100% at $+\infty$.

Determining the margin for intra-fractional breathing motion was a three-step process. First, the position of the prescribed isodose level was determined. In this step the dose

Table 1. Fitting parameters for equation (2) to describe a one-sided dose profile, with w the relative weight and b the slope in millimetres.

	w_1/w_2	b_1/b_2
Lung	0.6/0.4	5.0/18.0
Water	0.8/0.2	3.5/17.0

distribution could already have been blurred for random setup variations due to causes other than patient breathing, e.g., random setup errors having a Gaussian probability density function. Fitting the dose distribution with error functions allowed fast blurring by replacing the slope b of the error functions with $\sqrt{b^2 + 2\sigma^2}$ in which σ represents the standard deviation of the Gaussian PDF. Second, the dose distribution was blurred with the breathing PDF and again the position of IDL_{pres} was determined. The difference in location of IDL_{pres} determined the safety margin for intra-fractional breathing. Third, the breathing PDF was mirrored (positive displacements were made negative and vice versa) and the second step was repeated. This last step was performed because breathing PDFs are usually asymmetric, which will result in a non-equal shift of IDL_{pres} for the 'left-hand side' and 'right-hand side' penumbra, as already pointed out by, e.g., van Herk (2004). We chose the maximum displacement in IDL_{pres} to be the representative one.

3. Results

3.1. Base-line drift and irregular breathing

As mentioned earlier, both irregular breathing and base-line shifts during prolonged breathing may influence the shape of the breathing PDF. Especially the small peak that is expected at the inhale position of a PDF for which breathing motion is accurately described by a power of the cosine function, e.g. $\cos^4$, was often missing in our data. This may be because of base-line drifts or because it is more difficult for a patient to reproduce the exact same inhale position, i.e. irregular breathing amplitudes. Figure 3 shows breathing traces and corresponding PDFs for both examples as well as for regular breathing. It is expected that the less pronounced inhale peak will be lost more rapidly due to any smearing effects than the exhale peak. Even if each single breath adheres to a $\cos^{2n}$ fit, the PDF for multiple breaths does not have to do so.

Our measured PDFs showed a great variety of shapes, some of which loosely represented the PDF of breathing motion proportional with $\cos^{2n}$, but for just as many traces the PDF itself was almost Gaussian shaped. It was impossible to fit all PDFs with a simple function. This seems to prohibit the design of a simple margin recipe for intra-fractional breathing motion with the (median) peak-to-peak breathing amplitude as the only parameter. We investigated whether assuming the measured PDFs to be represented by a Gaussian distribution with a certain standard deviation, which is coupled to the peak-to-peak breathing amplitude, would allow construction of an accurate, but simple, margin recipe.

3.2. Dose profiles

Figure 4 shows the effect of breathing on the dose profile in material of lung density. The solid grey line represents the dose profile in the absence of intra-fractional breathing. The dashed black line is the same profile blurred with the breathing PDF. This PDF is displayed

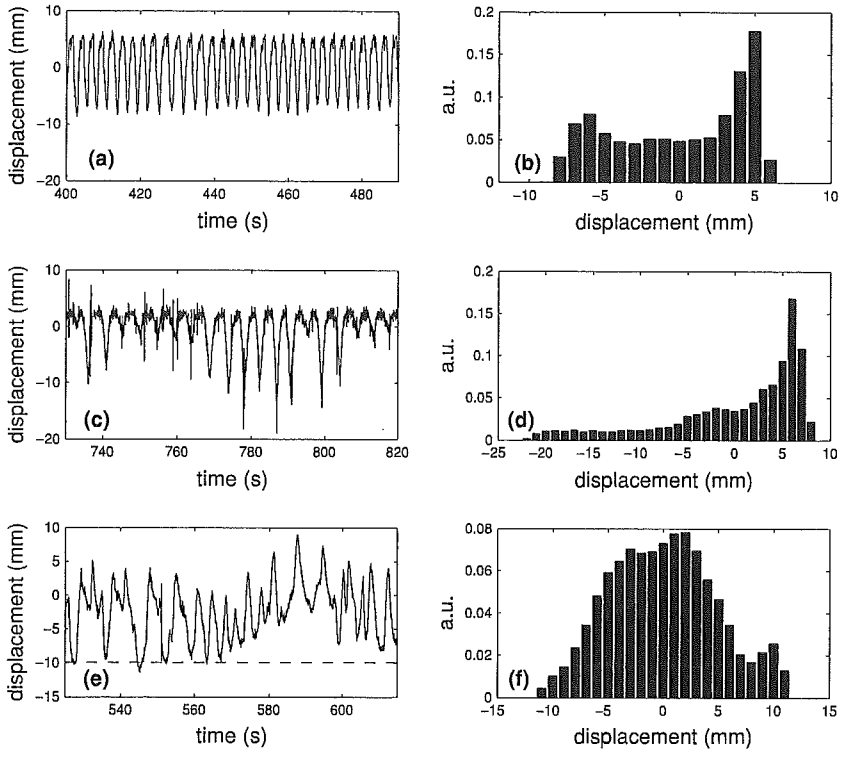

Figure 3. Ninety second sections of breathing traces and the PDF of the whole trace. Parts (a) and (b) represent regular breathing. Parts (c) and (d) represent an irregular breathing amplitude. Parts (e) and (f) represent a base-line drift, exemplified by the horizontal dashed line in (e). The data points were shifted to result in an average displacement of zero over the entire breathing trace.

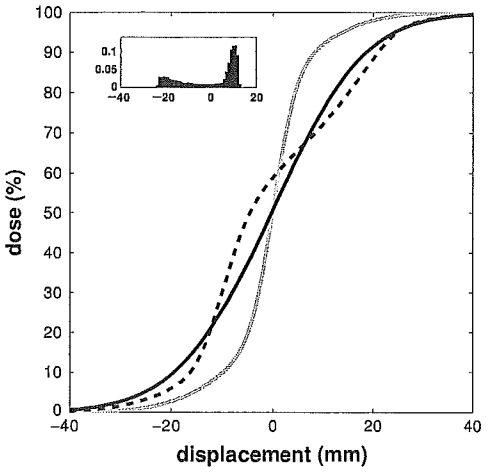

Figure 4. Dose profiles for an 8 MV penumbra in lung. The grey line is the unblurred profile which is either blurred with a breathing PDF (dashed black line) or with a Gaussian PDF with the standard deviation of the breathing PDF (solid black line). The inset shows the specific breathing PDF.

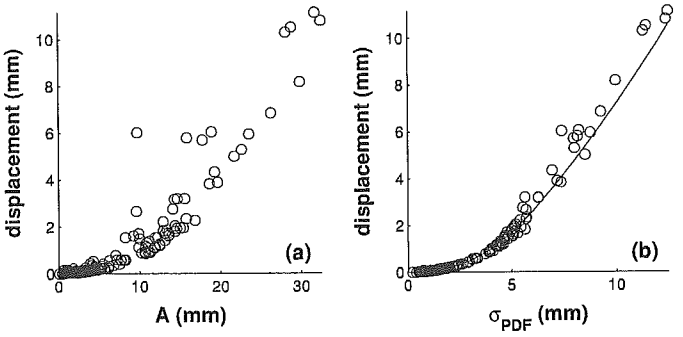

Figure 5. Additional displacement in the prescribed isodose level as a function of (a) the median breathing amplitude of the PDF, and (b) the standard deviation of the PDF. The data in the graphs are for a lung penumbra, an isodose level of 95% and a standard deviation of random setup errors of 0. The solid line in (b) represents the displacement for a Gaussian PDF with a standard deviation of σ_{PDF}.

in the inlay in upper left corner of the graph. The asymmetry of the breathing PDF results in an irregular dose profile after blurring. The solid black line is the result of blurring with a Gaussian PDF with the same standard deviation as the breathing PDF, σ_{PDF}. There is an obvious difference in the dose profiles after blurring, which indicates that a Gaussian PDF does not accurately model the effects of real breathing. However, the example shown in figure 4 is an extreme case. For 90% of the measured PDFs, the difference between the two blurred profiles is negligible, and only shows up when the median peak-to-peak breathing amplitude of the PDF is at least 20 mm. Furthermore, even though the blurred dose profiles in figure 4 differ, the change in position of the high dose levels, e.g. 90% and 95%, with respect to the unblurred profile is not significantly different. This indicates that, as far as the additional margin is concerned, intra-fractional breathing motion may perhaps be treated as being Gaussian.

3.3. Additional margin

Figure 5(a) shows the displacement in the 95% isodose level, a direct measure for the necessary margin for respiration-induced tumour motion, as a function of the median peak-to-peak breathing amplitude, A. The displacement naturally increases with increasing magnitude of breathing motion and shows a reasonable correlation with the mean breathing amplitude. A better correlation is observed when the displacement is plotted as a function of the standard deviation of the breathing PDF, σ_{PDF} (figure 5(b)). The reduced correlation in figure 5(a) may be explained by base-line drifting or irregular breathing. The effect of base-line drifting is that even though the median breathing amplitude is small, peak-to-peak motion (PTP_{PDF}) and standard deviation (σ_{PDF}) of the entire breathing trace, and therefore the additional shift in IDL_{pres}, may be substantial. Irregular breathing may have a similar effect. The most pronounced outlier in figure 5(a) at coordinates (10, 6) corresponds with the breathing trace depicted in figure 3(c).

Figure 5(b) shows a very nice correlation. Also shown in this graph is a line indicating the theoretical shift in the 95% isodose level. This theoretical shift expresses the additional shift as a function of a Gaussian PDF with a standard deviation equal to that of the standard deviation of the breathing PDF, σ_{PDF}. For values of σ_{PDF} less than about 5 mm, theory and practice are nearly coinciding. For larger values of σ_{PDF} a better fit is obtained if a small

Table 2. Multiplication factors for σ_{PDF} to determine the effective standard deviation, as a function of the penumbra prior to blurring and the prescribed isodose level (IDL_{pres}). For a standard deviation in random errors of $\sigma_{rs} = 0/\sigma_{rs} = 3$.

	Lung		Water	
IDL_{pres}	90%	95%	90%	95%
$\sigma_{PDF} < 5$ mm	1.01/1.00	1.00/1.01	1.08/1.07	1.00/1.03
$\sigma_{PDF} > 5$ mm	1.14/1.13	1.05/1.07	1.18/1.17	1.08/1.09

correction is made to the standard deviation of the assumed Gaussian PDF, i.e. the 'effective' standard deviation ($\sigma_{PDF,e}$) has a value of $1.05 * \sigma_{PDF}$. This value does, however, depend on the steepness of the penumbra (or dose gradient) before blurring as well as on the prescription isodose level that is chosen to be the representative one (table 2).

For relatively small intra-fractional breathing motion ($\sigma_{PDF} < 5$ mm or $A < \approx 15$ mm) the effective standard deviation is equal to σ_{PDF}, except for a dose gradient equal to the penumbra in unit-density tissue and a prescription isodose level of 90%. For intra-fractional breathing motion for which σ_{PDF} is larger than 5 mm, the effective standard deviation of the breathing PDF increases notably, even with a factor of almost 1.2 for IDL_{pres} equal to 90% and a penumbra as steep as for an 8 MV beam in water. The effective standard deviation of breathing motion in the case of a lung penumbra is smaller than or equal to $\sigma_{PDF,e}$ for a water penumbra, expressing the fact that blurring has a larger effect in the case of a steep dose gradient. Random setup errors decrease the steepness of the dose profile and it is therefore expected that the margin for respiration-induced tumour motion decreases when random setup errors are present. The data in table 2 support this reasoning, but pre-blurring with a clinically relevant standard deviation of $\sigma_{rs} = 3$ mm (Engelsman *et al* 2001), has only a small effect.

Although the necessary margin for intra-fractional breathing motion is highly correlated with, and can be predicted from, the standard deviation of the entire breathing PDF, this PDF is not a quantity that can be measured prior to treatment planning. This may therefore obstruct the design of patient specific safety margins. However, both time-resolved CT-scanning and fluoroscopy may *a priori* give a general 'feel' as to the median peak-to-peak amplitude of breathing motion for a specific patient. This, and the fact that our data show a reasonable correlation between σ_{PDF} and the median breathing amplitude (figure 6), should allow adequate patient-specific margin design. Also shown in figure 6 is a linear fit of the data. This fit is forced through the origin since a PTP_{PDF} of zero automatically means a σ_{PDF} of zero. A slightly better fit would be obtained by letting go of this constraint. Once again, some of the outliers can presumably be explained by base-line drifting.

Figure 6 and table 2 combined allow the reader to come up with the effective standard deviation of intra-fractional breathing motion, which can subsequently be quadratically added to other sources of random uncertainties. Combined with knowledge of systematic uncertainties and a margin recipe, this will result in a safety margin from CTV to PTV. In the case of IDL_{pres} of 95% and a lung penumbra, the effective standard deviation is 42% of the median peak-to-peak breathing motion, which is only marginally larger than the 36% one can calculate for breathing motion described by equation (1) with $n = 2$. Even for large breathing motion and a prescribed isodose level of 90%, the effective standard deviation of 0.46 is close to the 'ideal' case. For a more direct result, and also to show how large (or small) the required additional safety margin can be, we summarized data as a function of IDL_{pres}, penumbra gradient, and presumed standard deviation of random setup errors, σ_{rs}, in table 3.

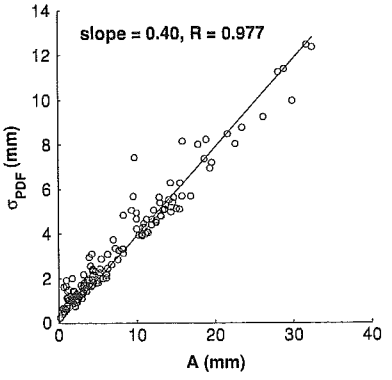

Figure 6. Standard deviation of the breathing PDFs as a function of the median peak-to-peak breathing amplitude of the breathing trace. The solid line is a best fit, forced through the origin.

Table 3. Margin for intra-fractional breathing motion as a function of the median peak-to-peak breathing amplitude, the penumbra of the dose distribution and the prescribed isodose level (IDL_{pres}). For a standard deviation in random errors of $\sigma_{rs} = 0/\sigma_{rs} = 3$.

		Lung		Water	
	IDL_{pres}	90%	95%	90%	95%
A	σ_{PDF}				
10	4	2.0/1.5	1.0/1.0	3.0/2.5	2.5/2.0
20	8	6.0/5.0	4.5/4.5	8.0/7.0	8.0/7.5
30	12	11.0/10.0	9.5/9.0	14.5/13.0	14.0/13.0

Table 3 and figure 5(a) clearly show that the margin for intra-fractional breathing motion is not linearly proportional with the peak-to-peak breathing amplitude. The necessary margin (or the allowed margin reduction) is only a few millimeters for a breathing amplitude of 10 mm or less, but increases rapidly with increasing breathing amplitude. Furthermore, as expected, the steeper dose gradient of a penumbra in water requires larger margins compared to a lung penumbra. For 30 mm peak-to-peak breathing motion and a water penumbra, the shift in IDL_{pres} is almost 15 mm. Since our margin reduction is one sided this means that the decrease in field diameter is equal to the peak-to-peak breathing motion, or the decrease in field radius is equal to the breathing amplitude. And this is only taking into account the blurring effect of breathing. If systematic effects of breathing, e.g. a non-representative CT-scan, are also taken into account, the total margin necessary for breathing will be larger than the amplitude of breathing, this in contrast to what van Herk (2004) and McKenzie (2000) reported. If the 90% isodose level is chosen to be the representative isodose level, table 3 shows that slightly larger margins are required than when coverage with the 95% isodose level is pursued. Apparently, isodose levels that are geometrically close to both the 'flat' high dose region and the steep penumbra are more sensitive to blurring.

4. Discussion

We evaluated the effect of intra-fractional breathing motion on the application of safety margins in photon radiotherapy. The results reported in this study can either be used to determine the

allowable reduction in margin between the CTV and PTV without loss of tumour control, if patient respiration during irradiation is controlled, or to determine the margin that needs to be applied, if not. To take into account the effects of base-line drifts and irregular patient breathing, we used patient breathing data as measured during RTRT as performed at the Hokkaido University Clinic. We would like to stress that our study is limited to the dose-blurring effect of intra-fractional breathing motion, and that we did not consider differences in positioning accuracy or systematic errors, which require their own margins.

4.1. Limitations of the study

Barring the use of image-guided radiotherapy during treatment delivery it is difficult to verify whether the amplitude of patient breathing, as assessed prior to treatment planning during fluoroscopy or time-resolved CT-scanning, is really characteristic or if the patient is an irregular breather, and unsafe margins may be applied. On the other hand, our study assumes that the dose gradient in a dose distribution is entirely determined by the penumbra of a single field or by the overlapping penumbra, e.g. the cranial and caudal edges of a target volume irradiated with a co-planar field setup. For other cases, any point in the dose distribution receiving the prescription isodose level may be in the penumbra of only a limited number of beams. In other words, a large part of the delivered dose (e.g. 60%) may be insensitive to intra-fractional breathing motion and instead of evaluating the shift in the 95% isodose level we should have been evaluating the shift in the 35% isodose level of a certain beam for that point. This isodose level may actually move outward due to blurring. For these cases, the numbers in this study should be taken as a worst case.

Our analysis intrinsically assumes that the dose distribution is insensitive to either setup uncertainties or respiration-induced changes in the density distribution within the patient. Both Engelsman *et al* (2001) and Beckham *et al* (2002) report limited changes in the photon dose distribution due to these causes. Furthermore, for IMRT plans there is an interplay effect between the motion of the MLC during treatment delivery and breathing motion (Yu *et al* 1998) which is disregarded in our study. However, recent studies indicate that in typically fractionated IMRT treatments the interplay effect on the dose distribution is small (e.g., Bortfeld *et al* 2002, Chui *et al* 2003, Jiang *et al* 2003), and the main effect is dose blurring (penumbra widening), like in conventional treatment techniques. Therefore, the main conclusions of this paper are valid for IMRT as well. In the case of lung tumours for which additional dose is delivered to the rim of the field to sharpen the beam penumbra (Dirkx *et al* 1999), probably our 'water' penumbra will provide a better estimate of the required increase in safety margins. The margins in table 3 are for an 8 MV beam. For other beam energies the margins may be slightly larger or smaller depending on the dose gradient prior to blurring being more steep (e.g. 6 MV) or more shallow (e.g. 18 MV).

4.2. Clinical implications

A number of treatment planning studies have been performed in which safety margins are reduced because of control of patient breathing. For hepatic tumours, Haken *et al* (1997) studied the effect of eliminating the 1 to 2 cm margin otherwise applied in the superior and inferior direction. The result was an NTCP decrease of about 4.5%, allowing a TCP increase by means of iso-NTCP dose escalation of about 6–7% (8 to 10 Gy). Wagman *et al* (2003) found an allowable increase in prescribed dose of about 20% because of margin reduction from 2 cm to 1 cm using RPM.

For lung tumours, Barnes *et al* (2001) showed a decrease in the lung volume receiving 20 Gy or more (V20) from 11.0% to 8.8% when using smaller margins because of DIBH. Hanley *et al* (1999) reduced the margin for lung treatments from 1–2 cm to 0.2–0.5 cm using a deep-inspiration breath-hold technique. Just the margin reduction reduced the V25 by 18%. The reduction is even larger when also taking into account the increase in lung volume, i.e. 30%. They furthermore make the interesting observation that the beam penumbra increases because of the decreased lung density. This requires a margin increase of about 1.5 mm (i.e. a similar margin as required for up to 10 mm of peak-to-peak breathing motion), which they claim is clinically negligible compared to margins applied for setup errors and residual organ motion. All studies mentioned above report a significant and clinically relevant decrease in NTCP and/or increase in tumour control. Although the exact reduction in margin as applied in these studies, especially as a function of patient-specific breathing motion, is unclear, the extent of margin reduction seems to be globally in agreement with the allowable reduction reported in our study. However, the one thing common between the studies mentioned above is that they evaluated patients with substantial respiration-induced tumour motion, i.e. a peak-to-peak breathing motion of more than 15 mm. Only 15 out of 176 of our breathing traces (<10%) had such large breathing motion.

It is questionable whether control of patient breathing during irradiation is practical for patients with limited breathing motion, i.e. less than 10 mm peak-to-peak. The 1 to 2 mm allowable reduction in margins near tumour–lung interfaces can easily be offset by a necessary increase in safety margins because of a small increase in other random uncertainties (like inter- and intra-fraction reproducibility of the frozen tumour position). Even a small additional systematic uncertainty may be introduced because of efforts to control patient breathing. Hanley *et al* (1999) report an inter- and intra-fraction reproducibility of 2.5 and 1.0 mm. The accuracy of external respiratory monitors is why, e.g. Mageras and Yorke (2004), do not reduce the safety margin even though they are using DIBH. Their reasons being that (1) as the lung expands, microscopic disease may expand as well, (2) expansion of the lung allows sufficient target dose escalation and (3) their dose calculation algorithm does not accurately model penumbra broadening due to the decrease in lung density. They furthermore state that, although image guidance is the treatment method of choice, it requires percutaneous marker insertion resulting in a significant chance of complications. We suggest selection at the gate in order to only control patient breathing during irradiation for those patients that have a large magnitude of breathing motion. This selection can, for example, be obtained by performing a fluoroscopy session. Tumor location, e.g. lower lobe tumours, may not necessarily correlate with a large magnitude of breathing motion (Sixel *et al* 2003, Stevens *et al* 2001).

4.3. Margin recipe

It is interesting to verify whether the margins as obtained in our study are in agreement with margin recipes as found in the literature (see the overview in van Herk (2004)). A recipe provided by van Herk *et al* (2000), stripped from the part describing the margin for systematic uncertainties, is

$$M = 1.64(\sigma - \sigma_p). \tag{3}$$

In which M is the margin, σ_p is the standard deviation of the penumbra and σ is the quadratic sum of standard deviations of all random uncertainties. The value of 1.64 corresponds with coverage of the target volume by the 95% isodose level.

Table 4 shows that our study is in excellent agreement with the mentioned margin recipe. The agreement is not surprising since their analysis also used a Gaussian penumbra. However,

Table 4. Application of the margin recipe described in equation (3). M_{br} and $M_{no\text{-}br}$ are the margin for blurring including and excluding intra-fractional breathing, respectively. All values are in mm.

	Lung density			Water density		
A	10	20	30	10	20	30
σ_{PDF}	4.0	8.0	12.0	4.0	8.0	12.0
$\sigma_{PDF,e}$	4.0	8.5	12.7	4.1	8.6	13.0
σ_{rs}	3.0	3.0	3.0	3.0	3.0	3.0
σ_{p}	11.0	11.0	11.0	4.0	4.0	4.0
M_{br}	1.8	5.3	10.0	4.0	9.8	16.2
$M_{no\text{-}br}$	0.7	0.7	0.7	1.6	1.6	1.6
Difference	1.1	4.6	9.3	2.4	8.2	14.6
Our study	1.0	4.5	9.5	2.5	8.0	14.0

our values for σ_p had to be tweaked. Looking at table 1 our values of 11 and 4 mm are not unrealistic when taking into account the relative weighting of the two error functions describing our penumbra. In accordance with van Herk (2004), our study also shows that a small uniform margin can be applied for tumour motion with peak-to-peak breathing motion of less than 10 mm. We would, however, suggest to use a standard deviation of $0.4A$ instead of $0.3A$ when adding breathing motion to random uncertainties. Our study shows that the margin depends on the local dose gradient. This means that, in essence, there is a circular dependence between the margin, the treatment plan design and the local dose gradient.

5. Conclusions

Our analysis of the effect of intra-fractional breathing motion on the margin that should be applied during radiotherapy has revealed that the said motion can be assumed to have a Gaussian probability density function with a standard deviation of about 0.4 times the peak-to-peak amplitude of breathing motion. Base-line drifts and irregular breathing can lead to underestimating the margin but, in clinical practice, this will happen only seldom. The margin depends on the local dose gradient and increases rapidly with increasing amplitude of breathing. For patients having a peak-to-peak tumour motion due to breathing of 10 mm or less, control of breathing motion during radiation delivery only allows a small reduction in safety margins. The benefit of this reduction has to be weighed against the effort needed to control the breathing motion, the possible introduction of other motion errors and the possible inconvenience for the patient.

Acknowledgments

The authors would like to thank Steve B Jiang for his useful insights and helpful suggestions.

References

Barnes E, Murray B, Robinson D, Underwood L, Hanson J and Roa W 2001 Dosimetric evaluation of lung tumour immobilization using breath hold at deep inspiration *Int. J. Radiat. Oncol. Biol. Phys.* **50** 1091–8

Beckham W, Keall P and Siebers J 2002 A fluence-convolution method to calculate radiation therapy dose distributions that incorporate random set-up error *Phys. Med. Biol.* **47** 3465–73

Berbeco R I, Jiang S B, Sharp G C, Chen G T, Mostafavi H and Shirato H 2004 Integrated radiotherapy imaging system (IRIS): design considerations of tumour tracking with linac gantry-mounted diagnostic x-ray systems with flat-panel detectors *Phys. Med. Biol.* **49** 243–55

Bortfeld T, Jokivarsi K, Goitein M, Kung J and Jiang S 2002 Effects of intra-fraction motion on IMRT dose delivery: statistical analysis and simulation *Phys. Med. Biol.* **47** 2203–20

Chui C-S, Yorke E and Hong L 2003 The effects of intra-fraction organ motion on the delivery of intensity-modulated field with a multileaf collimator *Med. Phys.* **30** 1736–46

Dirkx M, Essers M, van Sornsen de Koste J, Senan S and Heijmen B 1999 Beam intensity modulation for penumbra enhancement in the treatment of lung cancer *Int. J. Radiat. Oncol. Biol. Phys.* **44** 449–54

Engelsman M, Damen E, Jaeger K D, Ingen K v and Mijnheer B 2001 The effect of breathing and set-up errors on the cumulative dose to a lung tumour *Radiother. Oncol.* **60** 95–105

Ford E, Mageras G, Yorke E and Ling C 2003 Respiration-correlated spiral CT: a method of measuring respiratory-induced anatomic motion for radiation treatment planning *Med. Phys.* **30** 88–97

Haken R T, Balter J, Marsh L, Robertson J and Lawrence T 1997 Potential benefits of eliminating planning target volume expansions for patient breathing in the treatment of liver tumours *Int. J. Radiat. Oncol. Biol. Phys.* **38** 613–7

Hanley J *et al* 1999 Deep inspiration breath-hold technique for lung tumours: the potential value of target immobilization and reduced lung density in dose escalation *Int. J. Radiat. Oncol. Biol. Phys.* **45** 603–11

ICRU 1993 International Commission on Radiation and Measurements Units Report 50: Prescribing, recording, and reporting photon beam therapy *Technical Report* (Bethesda, MD: ICRU)

ICRU 1999 International Commission on Radiation and Measurements Units Report 62: Prescribing, recording, and reporting photon beam therapy (Supplement to ICRU Report 50) *Technical Report* (Bethesda, MD: ICRU)

Jiang S B, Pope C, Jarrah K M A, Kung J H, Bortfeld T and Chen G T Y 2003 An experimental investigation on intra-fractional organ motion effects in lung IMRT treatments *Phys. Med. Biol.* **48** 1773–84

Lagerwaard F, de Koste J V S, Nijssen-Visser M, Schuchhard-Schipper R, Oei S, Munne A and Senan S 2001 Multiple 'slow' CT scans for incorporating lung tumour mobility in radiotherapy planning *Int. J. Radiat. Oncol. Biol. Phys.* **51** 932–7

Lujan A, Larsen E, Balter J and Haken R T 1999 A method for incorporating organ motion due to breathing into 3D dose calculations *Med. Phys.* **26** 715–20

Mageras G S and Yorke E 2004 Deep inspiration breath hold and respiratory gating strategies for reducing organ motion in radiation treatment *Semin. Radiat. Oncol.* **14** 65–75

McKenzie A 2000 How should breathing motion be combined with other errors when drawing margins around clinical target volumes? *Br. J. Radiol.* **73** 973–7

Seppenwoolde Y, Shirato H, Kitamura K, Shimizu S, van Herk M, Lebesque J V and Miyasaka K 2002 Precise and real-time measurement of 3D tumour motion in lung due to breathing and heartbeat, measured during radiotherapy *Int. J. Radiat. Oncol. Biol. Phys.* **53** 822–34

Shirato H *et al* 2000 Four-dimensional treatment planning and fluoroscopic real-time tumour tracking radiotherapy for moving tumour *Int. J. Radiat. Oncol. Biol. Phys.* **48** 435–42

Shirato H, Seppenwoolde Y, Kitamura K, Onimura R and Shimizu S 2004 Intrafractional tumour motion: Lung and liver *Semin. Radiat. Oncol.* **14** 10–8

Shirato H, Shimizu S, Shimizu T, Nishioka T and Miyasaka K 1999 Real-time tumour-tracking radiotherapy *Lancet* **353** 1331–2

Sixel K E, Ruschin M, Tirona R and Cheung P C F 2003 Digital fluoroscopy to quantify lung tumour motion: potential for patient-specific planning target volumes *Int. J. Radiat. Oncol. Biol. Phys.* **57** 717–23

Stevens C, Munden R, Forster K, Kelly J, Liao Z, Starkschall G, Tucker S and Komaki R 2001 Respiratory-driven lung tumour motion is independent of tumour size, tumour location, and pulmonary function *Int. J. Radiat. Oncol. Biol. Phys.* **51** 62–8

van Herk M 2004 Errors and margins in radiotherapy *Semin. Radiat. Oncol.* **14** 52–64

van Herk M, Remeijer P, Rasch C and Lebesque J 2000 The probability of correct target dosage: dose-population histograms for deriving treatment margins in radiotherapy *Int. J. Radiat. Oncol. Biol. Phys.* **47** 1121–35

Vedam S, Keall P, Kini V, Mostafavi H, Shukla H and Mohan R 2003 Acquiring a four-dimensional computed tomography dataset using an external respiratory signal *Phys. Med. Biol.* **48** 45–62

Wagman R, Yorke E, Ford E, Giraud P, Mageras G, Minsky B and Rosenzweig K 2003 Respiratory gating for liver tumours: use in dose escalation *Int. J. Radiat. Oncol. Biol. Phys.* **55** 659–68

Wong J, Sharpe M, Jaffray D, Kini V, Robertson J, Stromberg J and Martinez A 1999 The use of active breathing control (ABC) to reduce margin for breathing motion *Int. J. Radiat. Oncol. Biol. Phys.* **44** 911–9

Yu C, Jaffray D and Wong J 1998 The effects of intra-fraction organ motion on the delivery of dynamic intensity modulation *Phys. Med. Biol.* **43** 91–104

Int. J. Radiation Oncology Biol. Phys., Vol. 61, No. 5, pp. 1559–1564, 2005

0360-3016/05/$–see front matter

ELSEVIER

doi:10.1016/j.ijrobp.2005.01.006

PHYSICS CONTRIBUTION

REAL-TIME MONITORING OF A DIGESTIVE TRACT MARKER TO REDUCE ADVERSE EFFECTS OF MOVING ORGANS AT RISK (OAR) IN RADIOTHERAPY FOR THORACIC AND ABDOMINAL TUMORS

TAKAYUKI HASHIMOTO, M.D.,*† HIROKI SHIRATO, M.D.,* MOTOTSUGU KATO, M.D.,‡ KOICHI YAMAZAKI, M.D.,§ NOBUAKI KURAUCHI, M.D.,¶ TOSHIAKI MORIKAWA, M.D.,‖ SHINICHI SHIMIZU, M.D.,* YONG CHAN AHN, M.D.# YASUYUKI AKINE, M.D.,† AND KAZUO MIYASAKA, M.D.*

Departments of *Radiology, ‡Division of Endoscopy, §First Internal Medicine, ¶First Surgery, and ‖Second Surgery, Hokkaido University School of Medicine, Sapporo, Japan; †Proton Medical Research Center and Department of Radiation Oncology, University of Tsukuba, Ibaraki, Japan; and #Department of Radiation Oncology, Samsung Medical Center, Surgkyunkwan University School of Medicine, Seoul, South Korea

Purpose: To evaluate the feasibility of real-time monitoring of a fiducial marker in/near the digestive tract and to analyze the motion of organs at risk to determine a reasonable internal margin.
Methods and Materials: We developed two methods to insert a fiducial marker into/near the digestive tract adjacent to the target volume. One method involves an intraoperative insertion technique, and the other involves endoscopic insertion into the submucosal layer of the normal digestive tract. A fluoroscopic real-time tumor-tracking radiotherapy system was used to monitor the marker.
Results: Fourteen markers (2 in the mediastinum and 12 in the abdomen) were implanted intraoperatively in 14 patients with no apparent migration. Seventeen of 20 markers (13/14 in the esophagus, 1/2 in the stomach, and 3/4 in the duodenum) in 18 patients were implanted using endoscopy without dropping. No symptomatic adverse effects related to insertion were observed. The mean/standard deviation of the range of motion of the esophagus was 3.5/1.8, 8.3/3.8, and 4.0/2.6 mm for lateral, craniocaudal and anteroposterior directions, respectively, in patients with intrafractional tumor motion less than 1.0 cm.
Conclusion: Both intraoperative and endoscopic insertions of a fiducial marker into/near the digestive tract for monitoring of organs at risk were feasible. The margin for internal motion can be individualized using this system. © 2005 Elsevier Inc.

Real-time tracking, Organ motion, Internal fiducial marker, Radiotherapy.

INTRODUCTION

Fluoroscopic real-time tumor-tracking radiotherapy system has been reported to be useful to minimize the internal margin for tumors in motion (1–12). However, even when we can place the tumor precisely, the position of the organ at risk (OAR) may be different from the planned position. If we can irradiate patients only when the OAR is *not* located in planning target volume, escalation of radiation dose or dose of antineoplasmic agent in chemoradiotherapy may be possible. We anticipated that real-time tracking of markers in OAR, not in the tumor, during the irradiation can minimize the dose to the OAR and minimize the risk of producing serious complications. This treatment strategy, real-time organ-avoiding radiotherapy (ROART), will be possible.

Initially, we developed techniques to insert a 2.0-mm fiducial marker in/near the digestive tracts and monitored the motion of the marker during irradiation. The aim of the present study was to evaluate the feasibility of real-time monitoring of a fiducial marker in/near the digestive tract and to analyze the motion of the OAR. The motion analysis will be useful also to determine a population-based internal margin of the OAR in conventional treatment.

METHODS AND MATERIALS

Fluoroscopic tracking and gated radiotherapy system

A fluoroscopic real-time tracking system was used to monitor the position of a metallic fiducial marker in or near the digestive tract. The details of the tracking system have been described previously (10–12). A 2.0-mm spherical gold (99.99% Au) marker was inserted into the OAR. The system consisted of 4 sets of

Reprint requests to: Takayuki Hashimoto, M.D., Proton Medical Research Center and Department of Radiation Oncology, University of Tsukuba, 1-1-1, Tennohdai, Tsukuba, Ibaraki, 305-8575, Japan. Tel: (+81) 29-853-7100; Fax: (+81) 29-853-7102; E-mail: hashimoto@pmrc.tsukuba.ac.jp

Received Aug 18, 2004, and in revised form Dec 28, 2004. Accepted for publication Jan 3, 2005.

diagnostic X-ray imaging equipment, image processor units, a trigger control unit, an image display unit, and a dual-photon conventional linear accelerator with multileaf collimators. The system was developed to determine the three-dimensional position of a metallic marker in the human body every 0.03 s by means of 2 of 4 sets of diagnostic fluoroscopy equipment to avoid blocking the X-ray images with the gantry of the linear accelerator. The linac is gated to irradiate the tumor only when the internal marker is located within the region of the planned coordinates relative to the isocenter.

In this study, the marker is implanted in the OAR and used as a reference for the position of the OAR. The discrepancy between the actual position of the marker in the OAR and its planned position can be monitored during irradiation every 0.03 s. When this discrepancy is larger than the permitted dislocation, the treatment beam turns off. The permitted dislocation can be determined anisotropically, so that the treatment beam is not turned off if the OAR moves away from its planned position but also away from the planning target volume.

The present tracking system can track only 1 marker during irradiation, so when the OAR marker is tracked during irradiation, the fiducial marker for the tumor cannot be used also for tumor tracking. Thus, the internal tumor margin cannot be reduced, and the internal margin for the OAR is reduced to 5 mm in this study.

In patients with markers inserted in both the tumor and OAR, tumor motion was monitored by tracking the marker inserted near the tumor using fluoroscopic systems on the first treatment day. If intrafractional motion of lung tumor was larger than 1.0 cm, ROART was not conducted for the patients, and they were treated with usual tumor tracking radiotherapy. Written consent was taken before the monitoring of the tumor motion of all the patients enrolled in this study. Simultaneous independent tracking of the tumor marker and OAR marker is beyond the scope of the present study.

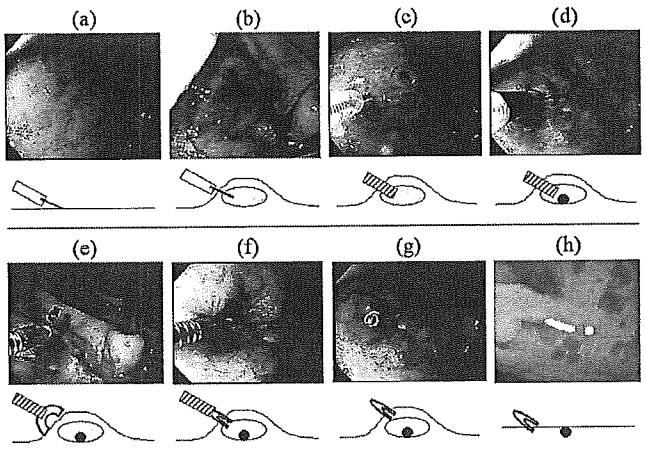

Fig. 1. The technical details of the insertion of the marker into the wall of the digestive tract. The photograph was taken during the experiment with the pig stomach. (a) Decide the position of insertion using endoscopy under fluoroscopic guidance. (b) Infuse physiologic saline into submucosal layer and lift the mucosal layer. (c) Insert the tip of the long needle to guide the marker. (d) Push out a gold marker into the submucosal space through the needle. (e, f, g) Close the entrance using metallic clip. (h) Check the position of the marker and the clip by X-ray fluoroscopy.

Insertion techniques

Endoscopic insertion technique. Animal experiments (Fig. 1): An endoscopic insertion technique was developed for a removed stomach of a pig using an electronic gastroduodenoscopy (GIF-Q240, Olympus, Tokyo, Japan). According to the technique of endoscopic mucosal resection for gastric neoplasms (13, 14), physiologic saline was injected into the submucosal space to lift the mucosa. A small incision in the lifted mucosal layer was performed with a needle knife to make a hole for the insertion of a gold marker. A special long needle (Olympus, Tokyo, Japan) has been made to insert the 2.0-mm gold marker through it. The needle is inserted through the endoscopy and has a enough length to reach the stomach. The needle is inserted into the submucosal space endoscopically, and then a gold marker is pushed out from the tip of the needle. After the insertion of the marker, the entrance hole of the mucosa is closed by fixation of a clip. The clip is made of light metal, so that the clip itself is not sufficient to be a fiducial marker. In other words, the clip does not interfere with the visualization of the gold marker. In this study, the procedure was judged as safe enough for clinical usage if 2 out of 3 trials were successful.

Clinical study: Patients with inoperable thoracic and abdominal tumors that were treatable with radiotherapy but were close to the digestive tract were candidates for endoscopic insertion. One or 2 markers were implanted for 1 patient. All candidates for endoscopic insertion were informed about the risk of the technique and the possibility of not gaining any benefit from this procedure. Written informed consent for the endoscopic procedure was given by all patients.

Intraoperative insertion technique. Clinical study: If a patient has a thoracic or abdominal tumor that is potentially partially unresectable, the surgeon brings a gold marker into the operating room before the operation. During the surgery, the marker is implanted near the unresectable tumors and near the OAR under the direction of the radiation oncologists to be used during ROART. We have made a bead, a 2.0-mm gold marker with a 0.5-mm pinhole, which can be fixed to the OAR by suturing the thread through the pinhole. Before the operation, written consent was given by the patients.

Clinical assessment

The day after the insertion of the marker, CT images were taken (Aquilion, Toshiba, Otawara, Japan) for treatment planning with a slice thickness and interval of 1.0 mm. In the protocol, the procedure would have been judged not to be justifiable if the markers dropped into the lumen of intragastrointestinal tract (drop) or migrated interstitially in the submucosal space (migration) from the implanted position in 2 out of initial 3 patients. If 1 of 3 patients experienced the drop/migration, the other 3 patients would be enrolled. If 2 of the initial 6 patients experienced drop/migration, the procedure would not have been justifiable. By using the stopping rule, the feasibility of the marker insertion technique was evaluated.

A confirmatory CT scan and/or plain X-ray images were taken periodically after the insertion for the assessment of the drop/migration of the marker. The drop of the marker was easily detected, but migration of the marker in the digestive tract was much more difficult to detect than in the liver or prostate (3). If the discrepancy between the marker and one adjacent anatomic structure was larger than 1 cm, 2 radiation oncologists measured several anatomic landmarks independently and judged the likelihood of migration.

Table 1. Patient characteristics

Disease	Patients (*n*)	Insertion	Marker position	Markers (*n*)	Drop/migration[§] (*n*)	Adverse event (*n*)
Lung cancer	12	Transendoscopic	Esophagus	10	1	1[‖]
		Intraoperative	Mediastinum	2	–	–
Esophageal cancer	3	Transendoscopic	Esophagus	4	–	–
Adrenal tumor*	1	Transendoscopic	Stomach	1	–	–
Gall bladder cancer	2	Intraoperative	Hepatic hilum	2	–	–
Bile duct cancer	9	Intraoperative	Hepatic hilum	9	–	–
Pancreas cancer	3	Intraoperative	Hepatic hilum	1	–	–
		Transendoscopic	Duodenum	2	1	–
			Stomach	1	1	–
Pancreas tumor[†]	1	Transendoscopic	Duodenum	1	–	–
Hepatic hilar lymph node[‡]	1	Transendoscopic	Duodenum	1	–	–

Metastasis from *colon cancer, [†]renal cancer, [‡]ovarian cancer.
[§]Number of the markers dropped/migrated from inserted position.
[‖]Asymptomatic ulcer (Common Terminology Criteria for Adverse Events v3.0 (CTCAE) Grade 1).

It was planned that all unexpected, serious adverse effects would be reported to the independent monitoring committees, consisting of institutional as well as noninstitutional members. Adverse acute reaction was classified according to the Common Terminology Criteria for Adverse Events (CTCAE) v3.0.

The motion of the esophagus and duodenum was evaluated using tracking data from real-time tumor-tracking radiotherapy system in this study to investigate the appropriate internal margin for OAR. The software used in this study is the same as in the previous series for lung tumors (6). In brief, data of coordinates of the marker during irradiation were used to measure range (maximum minus minimum) of the marker position. The range of the marker position was measured during a session of irradiation for each patient. Thus, the magnitude of the motion in this study included intrafractional but not interfractional baseline shift. We also measured the frequency of the main motion with the software used for lung (8) and liver (9) previously. In brief, a sinusoidal model of respiratory motion was used to calculate the frequency of the motion and was fitted to the actual data of the marker position (8).

RESULTS

An animal experiment

The marker was inserted into the submucosal space of a stomach of a pig by an endoscopic procedure on all 3 occasions. Endoscopists required 10–15 min for one procedure. The procedure was judged to be safe and feasible to be tried in clinical study.

Clinical study

In 18 patients, 20 markers were implanted into the submucosal layer using endoscopy (14 in the esophagus, 2 in

Table 2. Characteristics of patients with inserted marker(s) in esophagus

No.	Age/gender	Disease	Position	Drop/migration	Prescribed dose	Range of motion (mm) LR	CC	AP	Frequency (Hz)
1	63/M	Lung cancer	Ut	–	45 Gy/30 fr	3.9	8.4	2.3	0.32
2	74/M	Esophageal cancer*	Ut	–	64 Gy/32 fr	1.5	5.5	2.5	0.34
			Lt	–		3.6	9.9	5.4	NA
3	69/M	Lung cancer	Mt	–	40 Gy/20 fr	2.1	15.4	2.7	0.25
4	77/M	Lung cancer	Mt	–	60 Gy/30 fr	3.2	5.0	2.6	0.39
5	75/M	Lung cancer	Mt	–	66 Gy/33 fr	1.5	1.3	2.0	0.32
6	76/M	Lung cancer	Mt	–	65 Gy/26 fr	2.9	10.4	2.6	0.28
7	65/M	Lung cancer	Mt	–	45 Gy/30 fr	5.1	9.3	5.3	0.24
8	78/M	Lung cancer	Mt	–	60 Gy/30 fr	NA	NA	NA	NA
9	78/M	Lung cancer	Mt	–	40 Gy/16 fr	5.8	10.6	5.0	0.29
10	74/M	Esophageal cancer	Lt	–	66 Gy/33 fr	3.8	11.5	4.1	0.31
11	79/M	Lung cancer	Lt	–	46 Gy/23 fr	NA	NA	NA	NA
12	55/M	Esophageal cancer	Lt	–	60 Gy/30 fr	6.8	6.1	10.8	0.25
13	73/M	Lung cancer	Mt	Dropped[†]	66 Gy/33 fr	1.9	6.7	2.2	0.29

Abbreviations: Ut = upper thoracic esophagus; Mt = middle thoracic esophagus; Lt = lower thoracic esophagus; NA = not analyzable with the model; fr = fraction; LR = lateral; CC = craniocaudal; AP = anteroposterior.
* Double cancer.
[†] Reinsertion was performed.

the stomach, and 4 in the duodenum) (Table 1). Three patients with esophageal cancer for whom the marker was used for tumor tracking were included for this feasibility study. Sixteen out of the 18 (89%) patients did not experience drop/migration of the marker after the insertion. Three markers were dropped in 2 patients. One patient with lung cancer who received esophageal insertion experienced drop of the marker within a day after the insertion. Reinsertion was performed for the patient successfully. The other patient with pancreas cancer experienced dropping of 2 markers from stomach and duodenum within a week after the insertion.

No symptomatic adverse reactions related to insertion of the marker were reported. Asymptomatic ulcer of the esophagus (Grade 1) was observed in 1 patient as a result of minor mucosal injury during the endoscopic clipping procedure. This incident resulted in a 1-week delay in starting radiotherapy. Other patients received radiotherapy without an apparent delay in starting radiotherapy.

Twelve markers in 11 patients for whom esophageal insertion was successful were used to analyze the motion of the esophagus. The portion of the esophagus in which the marker was inserted was shown in Fig. 2. The mean/standard deviation of the range of motion (median, 95% confidence interval of the marker position) of the esophagus was 3.5/1.8 (3.2, 1.5–6.8) mm, 8.3/3.8 (8.4, 1.3–15.4) mm, and 4.0/2.6 (2.6, 2.0–10.8) mm for lateral (R-L), craniocaudal (C-C), and anteroposterior (A-P) directions, respectively (Table 2). The range of motion was the largest in the C-C direction in 9 patients, in the A-P direction in 2 patients, and in the R-L direction in none. There was a trend that motion of the marker was larger at the location below the level of the tracheal carina than at the upper location, but no statistical difference was demonstrated. Frequency was distributed from 0.24 to 0.39 Hz. Respiratory motion was the main source of the motion. Cardiac motion was also detected in the frequency analysis, but its magnitude was much smaller than that of respiratory motion (Fig. 3).

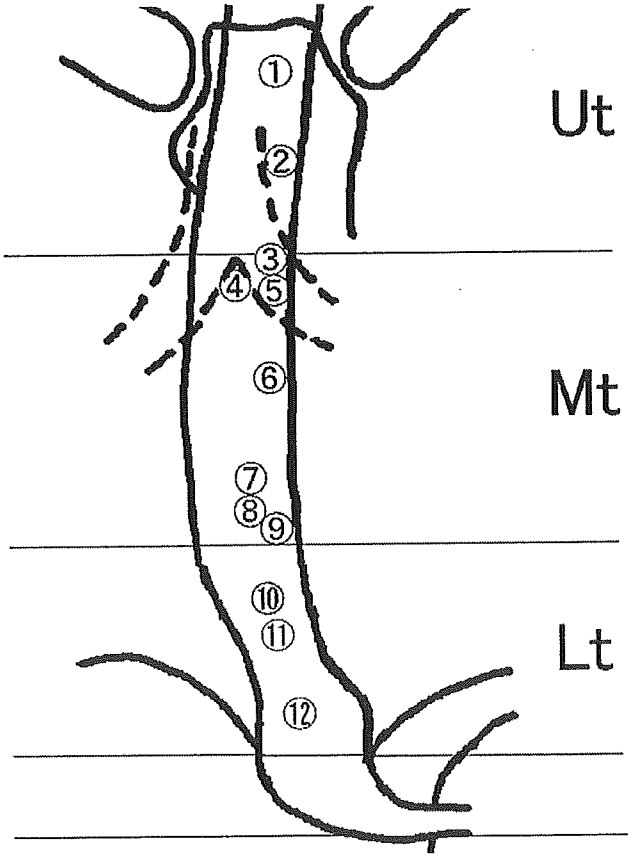

Fig. 2. Positions of 12 markers inserted into the esophagus in 11 patients to be used for motion analysis.

Table 3 shows characteristics of 4 patients for whom the marker was inserted into the duodenum. The median range of motion (95% confidence interval of the marker position) of the duodenum was 10.4 (6.8–11.6) mm, 22.2 (11.2–25) mm, and 10.5 (10.4–16.2) mm for the R-L, C-C, and A-P directions, respectively (Table 3).

Intraoperative insertion of the marker was performed in 14 patients; 12 patients with abdominal tumors and 2 patients with thoracic tumors. All patients experienced no drop of the marker. In two patients with mediastinal lymph node, the gold bead was successfully implanted near the tracheal carina using a video-assisted thoracotomy. The median range of motion was 3.6, 4.4, and 5.3 mm in 1 patient and 11.2, 2.7, and 2.2 mm in the other patient for the R-L, C-C, and A-P directions, respectively (Table 4). The frequency of the motion was 0.41 and 0.26 Hz, suggesting the respiratory motion was the main component of the movement.

As a whole, 30 (94%) out of 32 patients who received either endoscopic or intraoperative insertion experienced no drop/migration of the marker (Table 1). Follow-up CT scan

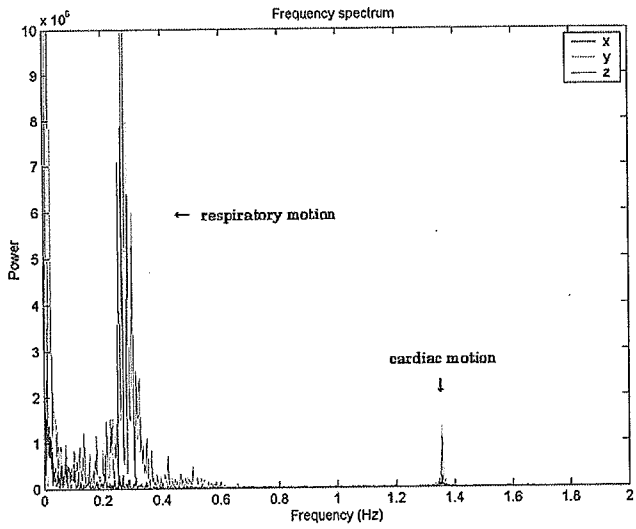

Fig. 3. Frequency analysis of movement of the marker inserted in the esophagus. The frequency spectrum of the lateral (R-L) (x), craniocaudal (CC) (y), and anteroposterior (A-P) (z) directions is displayed. There are two peaks in the frequency at 0.25 and 1.36 Hz. The higher peak is consistent with respiratory motion, and the lower peak is consistent with cardiac motion.

Table 3. Characteristics of patients with inserted marker in duodenum

No.	Age/gender	Disease	Drop/migration	Prescribed dose	Range of motion (mm)			Frequency (Hz)
					LR	CC	AP	
1	64/M	Pancreas cancer	Dropped	40 Gy/20 fr	–	–	–	–
2	74/F	Ovarian cancer*	–	60 Gy/30 fr	11.6	11.2	10.5	NA
3	75/M	Pancreas cancer	–	50.4 Gy/28 fr	10.4	22.2	10.4	0.17
4	73/M	Renal cancer†	–	50 Gy/25 fr	6.8	25.0	16.2	0.28

Abbreviations as in Table 2.
Metastatic *hepatic hilar lymph node, †pancreas cancer.

or plain X-ray film at least 1 month after the marker insertion was available in 30 (94%) of 32 patients. With the median follow-up of 10.0 (range, 1.1–48.0) months, the drop/migration rate at 3 months and 6 months after the insertion was 11.1 (3/27)% and 15 (3/20)%, respectively.

Because this was a feasibility study on marker insertion, the usual dose constraint was used for the organs at risk. No serious radiation-related adverse reaction Grade 3 or higher was noted with the median follow-up of 10.2 months.

DISCUSSION AND CONCLUSIONS

The digestive tract is one of the main OARs for many tumors undergoing radiotherapy. Reduction in treatment volume of these serial organs is critically important. One of the most difficult morbidities to overcome is esophagitis in areas of high-dose abdominal irradiation during chemoradiotherapy for lung cancer and for gastric and duodenal ulcer.

The introduction of an internal fiducial marker into the digestive tract may reduce the risk of complication resulting from high-dose irradiation to part of the digestive tract. This study shows that the insertion of the marker into submucosal space using the technique of endoscopic mucosal resection was feasible for the esophagus, stomach, and duodenum. Drop of the marker was seen only during the initial few days, as we have experienced also in lung study (5). The stability of the gold marker/bead after this period was reliable enough to be used in ROART. However, because we have used only 1 or 2 markers, rotation or distortion of the OAR cannot be detected. The uncertainty relating to this problem could be reduced if we were to insert 3 or more markers and measure the rotation angles (15).

A shortcoming of the present tracking system is that only 1 marker can be tracked and used for gating. Because the stomach and duodenum have complex, irregular shapes, one marker cannot represent the motion of the entire organ. The motion analysis in this study suggested that the motion of the duodenum had a mean range of 10, 22, and 11 mm in the R-L, C-C, and A-P directions, respectively. Our system may be useful only when the portion of duodenum that would be irradiated with a high dose is small enough to be represented by a few markers. The concepts of tomotherapy and the cone beam CT scanner are both expected to overcome this shortcoming of the fiducial marker system (16–18). However, real-time verification of the complex contour of these structures may still be difficult, because of the relatively large motion of the OAR.

Severe esophagitis is observed during chemoradiotherapy for locally advanced lung cancer (19, 20) and often causes interruption of the treatment. The motion analysis suggested that the internal margin should be determined to cover a mean range of 4, 8, and 4 mm of the esophagus in R-L, C-C, and A-P directions, respectively. The esophagus has simpler shape, and 1 marker may be useful for reducing severe esophagitis. A clinical protocol for a dose escalation study for lung cancer using this technique has been approved by our institutional ethical committee and has now opened.

Simultaneous tracking of the marker near the tumor and markers in the OAR may be much more difficult than we expect. Because we have not included the patients with intrafractional tumor motion larger than 1.0 cm, the measured motion may be different if the organ motion is dependent on the tumor motion. Aspects of the intrafractional motion of the OAR are likely to be independent of the motion of the tumor-containing organ, such as lung and liver. The dynamic control of the multileaf collimator with

Table 4. Characteristics of patients with inserted marker in mediastinum

No.	Age/gender	Disease	Drop/migration	Prescribed dose	Range of motion (mm)			Frequency (Hz)
					LR	CC	AP	
1	63/M	Lung cancer*	–	65 Gy/26 fr	3.6	4.4	5.3	0.41
2	52/M	Lung cancer*	–	35 Gy/4 fr	11.2	2.7	2.2	0.26

Abbreviations as in Table 2.
* Mediastinal lymph node recurrence.

real-time tumor tracking may compensate for this purpose (21, 22).

In conclusion, endoscopic and intraoperative insertion of a fiducial marker into the digestive tract was feasible and useful for measuring the motion of the OAR. The motion analysis suggested that the internal margin should be determined to cover a mean range of 4, 8, and 4 mm for the esophagus and 10, 22, and 11 mm for the duodenum in the R-L, C-C, and A-P directions, respectively. Real-time monitoring of the fiducial marker in the digestive tract may be useful for reducing the adverse reaction to thoracic and abdominal chemoradiotherapy.

REFERENCES

1. Kitamura K, Shirato H, Shinohara N, *et al.* Reduction in acute morbidity using hypofractionated intensity-modulated radiation therapy assisted with a fluoroscopic real-time tumor-tracking system for prostate cancer: Preliminary results of a phase I/II study. *Cancer J* 2003;9:268–276.
2. Shimizu S, Shirato H, Kitamura K, *et al.* Use of an implanted marker and real-time imaging for the positioning of prostate and bladder cancers. *Int J Radiat Oncol Biol Phys* 2000;48: 1591–1597.
3. Kitamura K, Shirato H, Shimizu S, *et al.* Registration accuracy and possible migration of internal fiducial gold marker implanted in prostate and liver treated with real-time tumor-tracking radiation therapy (RTRT). *Radiother Oncol* 2002;53: 1117–1123.
4. Onimaru R, Shirato H, Aoyama H, *et al.* Calculation of rotational setup error using the real-time tracking radiation therapy (RTRT) system and its application to the treatment of spinal schwannoma. *Int J Radiat Oncol Biol Phys* 2002;54: 939–947.
5. Shirato H, Harada T, Harabayasi T, *et al.* Feasibility of insertion/implantation of 2.0-mm-diameter gold internal fiducial markers for precise setup and real-time tumor tracking in radiotherapy. *Int J Radiat Oncol Biol Phys* 2003;56:240–247.
6. Shimizu S, Shirato H, Ogura S, *et al.* Detection of lung tumor movement in real-time tumor-tracking radiotherapy. *Int J Radiat Oncol Biol Phys* 2001;51:304–310.
7. Harada T, Shirato H, Ogura S, *et al.* Real-time tumor-tracking radiation therapy for lung carcinoma by the aid of insertion of a gold marker using bronchofiberscopy. *Cancer* 2002;95:1720–1727.
8. Seppenwoolde Y, Shirato H, Kitamura K, *et al.* Precise and real-time measurement of 3D tumor motion in lung due to breathing and heartbeat, measured during radiotherapy. *Int J Radiat Oncol Biol Phys* 2002;53:822–834.
9. Kitamura K, Shirato H, Seppenwoolde Y, *et al.* Tumor location, cirrhosis, and surgical history contribute to tumor movement in the liver, as measured during stereotactic irradiation using a real-time tumor-tracking radiotherapy system. *Int J Radiat Oncol Biol Phys* 2003;56:221–228.
10. Shirato H, Shimizu S, Shimizu T, *et al.* Real-time tumour-tracking radiotherapy. *Lancet* 1999;353:1331–1332.
11. Shirato H, Shimizu S, Kitamura K, *et al.* Four-dimensional treatment planning and fluoroscopic real-time tumor tracking radiotherapy for moving tumor. *Int J Radiat Oncol Biol Phys* 2000;48:435–442.
12. Shirato H, Shimizu S, Kunieda T, *et al.* Physical aspects of a real-time tumor tracking system for gated radiotherapy. *Int J Radiat Oncol Biol Phys* 2000;48:1187–1195.
13. Deyhle H, Sulser H, Säuberli H. Endoscopic snare ectomy of an early gastric cancer: A therapeutical method. *Endoscopy* 1974;6:195–198.
14. Tada M, Murata M, Murakami F, *et al.* Development of strip biopsy (summary in English). *Gastroenterol Endosc* 1984;26: 833–839.
15. Shirato H, Oita M, Fujita K, *et al.* Three-dimensional conformal set-up (3D-CSU) of the patients using the coordinate system provided by three internal fiducial markers and two orthogonal diagnostic X-ray systems in the treatment room. *Int J Radiat Oncol Biol Phys* 2004;60:607–612.
16. Mackie TR, Balog J, Ruchala K, *et al.* Tomotherapy. *Semin Radiat Oncol* 1999;9:108–117.
17. Mackie TR, Holmes T, Swerdloff S, *et al.* Tomotherapy: A new concept for the delivery of dynamic conformal radiotherapy. *Med Phys* 1993;20:1709–1719.
18. Jaffray DA, Siewerdsen JH, Wong JW, *et al.* Flat-panel cone-beam computed tomography for image-guided radiation therapy. *Int J Radiat Oncol Biol Phys* 2002;53:1337–1349.
19. Komaki R, Scott C, Lee JS, *et al.* Impact of adding concurrent chemotherapy to hyperfractionated radiotherapy for locally advanced non-small cell lung cancer (NSCLC): Comparison of RTOG 83–11 and RTOG 91–06. *Am J Clin Oncol* 1997; 20:435–440.
20. Langer CJ, Hsu C, Curran W, *et al.* Do elderly patients (pt) with locally advanced non-small cell lung cancer (NSCLC) benefit from combined modality therapy? A secondary analysis of RTOG 94–10. *Int J Radiat Oncol Biol Phys* 2001;51: 20–21.
21. Neicu T, Shirato H, Seppenwoolde Y, *et al.* Synchronized moving aperture radiation therapy (SMART): Average tumour trajectory for lung patients. *Phys Med Biol* 2003;48:587–598.
22. Sharp GC, Jiang SB, Shimizu S, *et al.* Prediction of respiratory tumor motion for real-time image-guided radiotherapy. *Phys Med Biol* 2004;49:425–440.

ELSEVIER

Int. J. Radiation Oncology Biol. Phys., Vol. 62, No. 4, pp. 1232–1238, 2005

0360-3016/05/$–see front matter

doi:10.1016/j.ijrobp.2005.03.039

PHYSICS CONTRIBUTION

COMPARISON OF IMAGING MODALITIES FOR THE ACCURATE DELINEATION OF ARTERIOVENOUS MALFORMATION, WITH REFERENCE TO STEREOTACTIC RADIOSURGERY

HIDEFUMI AOYAMA, M.D., PH.D.,* HIROKI SHIRATO, M.D., PH.D.,* NORIO KATOH, M.D.,* KOHSUKE KUDO, M.D., PH.D.,* TAKESHI ASANO, M.D., PH.D.,* SATOSHI KURODA, M.D., PH.D.,† TATSUYA ISHIKAWA, M.D., PH.D.,† AND KAZUO MIYASAKA, M.D., PH.D.*

Departments of *Radiology and †Neurosurgery, Hokkaido University Graduate School of Medicine, Sapporo, Japan

Purpose: To investigate the discrepancy between the arteriovenous malformations seen on magnetic resonance angiography (MRA) and on stereotactic digital subtracted angiography (DSA).
Methods and Materials: The target volume on stereotactic DSA (V_{DSA}) and the target volume on MRA (V_{MRA}) were separately delineated in 28 intracranial arteriovenous malformations. The coordinates of the center and the outer edges of V_{DSA} and V_{MRA} were calculated and used for the analyses.
Results: The standard deviations (mean value) of the displacement of centers of V_{MRA} from V_{DSA} were 2.67 mm (−1.82 mm) in the left-right direction, 3.23 mm (−0.08 mm) in the anterior-posterior direction, and 2.16 mm (0.91 mm) in the craniocaudal direction. V_{MRA} covered less than 80% of V_{DSA} in any dimensions in 9 cases (32%), although no significant difference was seen in the target volume between each method, with a mean value of 11.9 cc for V_{DSA} and 12.3 cc for V_{MRA} ($p = 0.948$).
Conclusion: The shift of centers between each modality is not negligible. Considering no significant difference between V_{DSA} and V_{MRA}, but inadequate coverage of the V_{DSA} by V_{MRA}, it is reasonable to consider that the target on MRA might include the feeding artery and draining vein and possibly miss a portion of the nidus.

Radiosurgery, Arteriovenous malformation, Magnetic resonance angiography, Computed tomography angiography, Angiography, Image guided radiation therapy.

INTRODUCTION

Stereotactic radiosurgery of brain lesions requires precise information on the target coordinates and morphology for single or fractionated high-dose application. For treatment planning of intracranial arteriovenous malformations (AVMs), stereotactic angiography has been the basic source of three-dimensional (3D) information of target volume (1–5). However, stereotactic angiography with the conventional biplanar technique is limited in its depiction of the 3D anatomy of AVMs (1). Recent improvements in conformal radiation techniques, such as 3D conformal radiation therapy and intensity-modulated radiation therapy, have made it possible to confine the high-dose radiation region to the 3D shape of the target. Because of this, a more precise 3D target shape is now required for radiosurgical planning. Gadolinium-enhanced 3D time-of-flight magnetic resonance angiography (MRA) and computed tomographic angiography (CTA) are the imaging modalities that can provide detailed 3D information on the AVM shape (3–12). However, discrepancies are frequently experienced between the target created on an MRA or CTA and the target on stereotactic angiography (5). The authors of previous publications have attributed the cause of this discrepancy to the poor depiction of AVM on biplanar stereotactic angiography (1, 3–11); however, none of these publications compared the targets created only on an MRA with those created only on a stereotactic angiography. In this study, therefore, we compared the target created on an MRA with the target created on a stereotactic angiography, to investigate the possible cause of the discrepancy between these two modalities. The feasibility of the use of CTA with a rapid injection contrast medium from the artery was also evaluated.

METHODS AND MATERIALS

The patients in this study consisted of 26 consecutive patients with intracranial pial AVMs treated between April 2002 and

Reprint requests to: Hidefumi Aoyama, M.D., Ph.D., Department of Radiology, Hokkaido University Graduate School of Medicine, North-15 West-7, Sapporo, Japan, 060-8638. Tel: (+81) 11-716-1161; Fax: (+81) 11-706-7876; E-mail: hao@radi.med.hokudai.ac.jp

Presented in part at the Annual Meeting of the American Society for Therapeutic Radiology and Oncology (ASTRO), Oct 18–23, 2003, Salt Lake City, UT.

Received Aug 2, 2004, and in revised form Mar 7, 2005. Accepted for publication Mar 9, 2005.